RSC Advances

PAPER

View Article Online
View Journal | View Issue

Cite this: *RSC Adv.*, 2018, **8**, 40813

Self-assembly of 2D-metal–organic framework/graphene oxide membranes as highly efficient adsorbents for the removal of Cs^+ from aqueous solutions†

Junye Cheng,‡[ab] Jie Liang,‡[ac] Liubing Dong,[d] Jixing Chai,[e] Ning Zhao,[b] Sana Ullah,[f] Hao Wang,*[b] Deqing Zhang,[e] Sumair Imtiaz,[f] Guangcun Shan*[a] and Guangping Zheng*[f]

The potential toxicity and irreversibility of radionuclide Cs place severe pressure on the natural environment, which has become one of the most forefront pollution problems in nuclear energy utilization. To solve this problem, novel self-assembled membranes consisting of two-dimensional (2D) metal–organic frameworks (MOFs) and graphene oxide (GO) were prepared by a facile filtration method, which can efficiently absorb Cs^+ from aqueous solutions. The batch experimental results showed that the sorption of Cs^+ on the GO/Co-MOF composite membrane was strongly dependent on the addition mass and the membrane compositions. Thus, the dominant interaction mechanism was interface or surface complexation and electrostatic interaction. The maximum sorption efficiency of Cs^+ on GO/Co-MOF was 88.4% with 8 mg addition mass at pH = 7.0 and 299 K. Detailed FT-IR and XPS analyses suggested that the efficient synergistic effects in the unique architectures of GO/Co-MOF play an important role in the high sorption capacity of Cs^+. The facile preparation method and the highly-efficient Cs^+ removal behaviour of GO/Co-MOF make the novel membrane a promising candidate for the elimination of radionuclide contamination.

Received 10th October 2018
Accepted 26th November 2018

DOI: 10.1039/c8ra08410f

rsc.li/rsc-advances

1. Introduction

With the huge development of global nuclear energy industry and projects, cesium (Cs) as a strategic resource plays an increasingly important role, which attracts a wide range of research interest.[1,2] However, large amounts of Cs ions are inevitably released into the natural environment.[1] Because of the long half-life time ($t_{1/2}$ = 30.17 years), strong γ radiation, high solubility and mobility of Cs^+ in the environment, particular attention has been paid to its separation and removal from aquatic environments especially after the disastrous accident at the Fukushima Daiichi nuclear power station in Japan.[3] Therefore, there is an urgent need to develop a highly efficient method for the removal of Cs^+ from waste streams before its intended long-term storage. A number of technologies for the capture of Cs^+ from wastewater have been reported in the past few decades, such as solvent extraction, ion exchange, co-precipitation, and adsorption processes.[4–7] Among the above-mentioned technologies, the adsorption process is widely applied in wastewater treatment owing to its simplicity, economy, good selectivity, and high efficiency.[8–13] In addition, the adsorbents can be easily regenerated during reversible adsorption. To achieve the rapid and efficient removal of Cs^+ from aqueous solutions, it is crucial to search for a suitable adsorbent with fast reaction rate and high sorption capacity, which also avoid aggregation in the adsorption processes.

Recently, metal–organic frameworks (MOFs) built from metal ions/clusters and organic linkers have drawn a lot of attention.[14] MOFs exhibit large pores and cavities in the range of molecular dimensions. Their pore size, connectivity and dynamic interaction with targeted guest molecules can be regulated by the judicious selection of organic and inorganic building blocks among a virtually unlimited number of

[a]*School of Instrumentation Science and Opto-electronics Engineering, Beihang University, No. 37 XueYuan Road, Beijing 100083, China. E-mail: gcshan@buaa.edu.cn*

[b]*Guangdong Provincial Key Laboratory of Micro/Nano Optomechatronics Engineering, College of Mechatronics and Control Engineering, Shenzhen University, Shenzhen 518060, China*

[c]*School of Space and Environment, Beihang University, No. 37 XueYuan Road, Beijing 100083, China. E-mail: whao@szu.edu.cn*

[d]*Graduate School at Shenzhen, Tsinghua University, Shenzhen 518055, China*

[e]*School of Materials Science and Engineering, Qiqihar University, Qiqihar 161006, China*

[f]*Department of Mechanical Engineering, Hong Kong Polytechnic University, Hung Hom, Kowloon, Hong Kong. E-mail: mmzheng@polyu.edu.hk*

† Electronic supplementary information (ESI) available. See DOI: 10.1039/c8ra08410f

‡ These authors contributed equally.

possibilities.[15–18] These properties endow MOFs a promising candidate for efficient removal of Cs^+ from aqueous solutions.[17] Several MOFs, such as HKUST-1 and MIL-101, were employed as adsorbents and their ability to remove Cs^+ from aqueous solution was studied.[19,20] Previous results indicated that the untreated MOFs showed limited adsorption capacity for Cs^+, and therefore they have to be functionalized by functional groups (Fe_3O_4/KNiFC or $-SO_3H$) to improve their affinity toward Cs^+. The additional steps not only complicated the synthetic procedure, but also increased the synthetic cost. In this work, we report the fabrication of flexible two-dimensional (2D) metal–organic framework (MOF)/graphene oxide (GO) composite membranes (GO/Co-MOF) through suction filtration of electrostatic self-assembly sheets consisting of intrinsically electronegative GOs and electropositive MOFs. The free-standing GO/Co-MOF membranes not only exhibit mechanical flexibility, but also perform well under severe conditions, such as immersing in strong acid/alkali aqueous solution. Herein, we investigated the Cs^+ removal capabilities of the GO/Co-MOF composite membranes in aqueous solutions. The Cs^+ removal experiments are carried out at varying contact times, reaction temperatures, concentrations, and different Co-MOF addition amounts.

2. Experimental

2.1 Materials

Graphite powder (<40 microns, synthetic), potassium permanganate ($KMnO_4$, 99.3%), sulfuric acid (H_2SO_4, 95–98%), cobalt nitrate hexahydrate ($Co(NO_3)_2 \cdot 6H_2O$, 98%), nickel nitrate hexahydrate ($Ni(NO_3)_2 \cdot 6H_2O$, 98%), polyvinylpyrrolidone (PVP, average mol wt 40 000), 4,4′-bipyridine (BPY), and *N*,*N*-dimethylformamide (DMF, 99.8%) were purchased from Sigma-Aldrich. Hydrochloric acid (HCl, 35.0–37.0%), hydrogen peroxide (H_2O_2, 30.0–35.5%), sodium nitrates ($NaNO_3$, 98.0%) were purchased from SAMCHUN. 5,10,15,20-tetrakis(4-carboxylphenyl)-porphyrin (TCPP, 97%) was purchased from Tokyo Chemical Industry Co. Ltd. Ethanol was purchased from Merck. An organic membrane filter (47 mm in diameter, Anodisc, Whatman) with a pore size of 0.25 μm was used for the preparation of the pristine and composite membranes through vacuum filtration processes. The deionized water was obtained from the Milli-Q System. All the chemicals were used as received without further purification.

2.2 Preparation of GO

In a typical procedure, GO was chemical exfoliated from natural graphite flakes *via* a modified Hummers method as reported in our previous research.[21] Typically, graphite flakes (5.0 g) and sodium nitrates (2.5 g) were put into concentrated sulfuric acid (115 mL) at room temperature. The mixture was under ice bath for 25 min with mild agitation. Potassium permanganate (15.0 g) was added gradually and the temperature of suspension was kept to below 10 °C for another 25 min. Then, the mixed suspension was heated to 35 °C and kept for 45 min until a thick paste was formed. Deionized water (140 mL) was added and the temperature of the solution was kept at 98 °C for 45 min. When the brown mixture turned into yellow, the mixture solution was diluted to 700 mL, followed by adding 30 mL H_2O_2 (30%). The mixture was then filtered and washed with 50 mL of HCl solution. Finally, the solution was centrifuged for several times at 11 000 rpm until the pH of the system was about 7. The resulting sample was dried in vacuum at 60 °C for 72 hours. 1 mg mL^{-1} of GO solution was prepared by the sonication of 1.1 g graphite oxide in 1 L DMF for about 2 hours, after which the aggregates were removed by mild centrifugation (3000 rpm for 10 min). The resulting dispersion was ready for further application.

2.3 Preparation of Co-MOF nanosheets and assembled 2D GO/Co-MOF composite membranes

$Co(NO_3)_2 \cdot 6H_2O$ (4.4 mg), BPY (1.56 mg) and PVP (10.0 mg) were dissolved in 6 mL of the mixture of DMF and ethanol (v/v = 3 : 1) in a 10 mL vial. Then the TCPP (4.0 mg) dissolved in 2 mL of the mixture of DMF and ethanol (v/v = 3 : 1) was added dropwise into the aforementioned solution, which was then sonicated for 25 min. After that, the vial was capped and then heated to 80 °C. After the reaction was kept for 24 h, the resulting red product was washed twice with ethanol and collected by centrifuging at 8000 rpm for 10 min. Finally, the 2D Co-MOF sheets were obtained, which were re-dispersed in DMF. The GO/Co-MOF composite membranes were prepared through an electrostatic self-assembly process. Typically, the dispersed GO suspension in DMF (1 mg mL^{-1}) was added into 20 mL of MOF (Co-MOF) suspension (1 mg mL^{-1}) drop by drop under stirring. Then the mixture was subjected to continuous magnetic stirring for 1 h. In the next step, the uniformly mixed GO and Co-MOF solution was filtered with organic membrane filters under vacuum. After filtration, the samples was peeled off from the organic membrane and dried for 24 hours in a vacuum oven at 60 °C. The Co-MOF based membrane was denoted as GO/2D-Co-MOF-*x*, where *x* was the mass percentage of Co-MOF in the composite. For comparison, GO membrane was prepared without the addition of MOF.

2.4 Adsorption experiments

The Cs^+ adsorption experiments for the GO/Co-MOF membranes were performed by a batch technique. The adsorbents were equilibrated with 10 mL of Cs^+ aqueous solution in stoppered glass tubes on a thermostat rotary shaker. The mixture was mechanically agitated at 240 rpm. After the predetermined time, the sorbents were separated from aqueous solution by filtering. And the concentration of cesium in the solution was measured by ICP. A series of adsorbents with different weights (2, 4, 6, 8 mg) were studied for the Cs^+ uptake. The effect of temperature on the adsorption capacity was evaluated at 299, 303, 313 and 323 K, respectively. The kinetics of adsorption process was investigated between 10 and 240 min at 299 K. Keeping other conditions unchanged, GO/Co-MOF membranes with different concentrations were also compared for the Cs^+ adsorption capacity. The cesium uptake quantity q_e (mg g^{-1}), expressed as the amount of cesium removed per unit

mass of the adsorbent is calculated according to the following equation:

$$q_e = \frac{(C_0 - C_e)V}{m} \quad (1)$$

where C_0 and C_e are initial and final concentrations (mg L^{-1}), respectively, m is the amount of the adsorbent (g) and V is the volume of the solution (L).

The removal efficiency, RE (%), was determined according to the following equation:

$$RE = \frac{C_0 - C_e}{C_0} \times 100\% \quad (2)$$

2.5 Characterization

Structural and phase characterizations of the as-prepared solid membranes were performed by XRD using a Bruker D2 Phaser diffractometer with Cu Kα irradiation ($\lambda = 1.54$ Å). The surface morphology of those samples was characterized by an environmental scanning electron microscope (ESEM, FEI/Philips XL30). The morphology and microstructure of the samples were revealed by a JEOL-2001F field-emission TEM. Tapping mode atomic force microscopy (AFM) measurement was performed with Nanoscope V controller (Veeco) equipped with an E-type vertical engage scanner at room temperature. The X-ray photon spectroscopy (XPS) examinations were carried out with a Sigma Probe and monochromatic X-ray source (XPS, K-Alpha, Thermo Scientific) to analyze the elemental compositions. The Raman spectroscopy technique (Renishaw) was used to analyze the structural information with 532 nm Nd:Yag laser.

3. Results and discussion

Single GO and Co-MOF nanosheets were presumably produced and characterized. GO nanosheets with various sizes were prepared by chemical exfoliation of graphite *via* a modified Hummers method.[21] Fig. 1a shows that the average size of GO sheets was 8–9 μm. The height profile of GO sheets with a thickness of ~1.1 nm verifies the exfoliation results in monolayer graphene oxides (Fig. S1a†). The complete exfoliation of graphite is further evidenced by the XRD patterns of GO with a sharp diffraction peak at $2\theta = 11.3°$ (Fig. S1b†).[22] Co-MOF nanosheets were prepared by a solvent thermal method. As shown in Fig. 1b, S2b and S2c,† the obtained Co-MOF present square-like nanosheet structure with a lateral dimension of ~8 μm. The corresponding synthesis mechanism is schematically shown in Fig. S1a.† Some overlapping parts among Co-MOF nanosheets were observed as shown in Fig. S2b† and a separated Co-MOF sheet is displayed in Fig. S2c.† It is noted that the diffraction ring and weak spots are observed in the selected area electron diffraction (SAED) pattern for Co-MOF nanosheet (Fig. S2d†), which suggests that Co-MOF is likely amorphous or weakly crystalline. Actually, even if the square-like Co-MOF nanosheet is crystalline, it may easily decompose under the highly powerful electron beam, and thus it is difficult to observe some diffraction spots in the SAED patterns.[23] The XRD patterns (Fig. S2e†) indicate that the Co-MOF is crystalline and exhibits a tetragonal structure. Energy-dispersive X-ray spectrometry (EDX) was also applied to reveal the structure of Co-MOF through the mapping analysis of elements C, N, and Co. As clearly shown in Fig. 1c, unambiguously, a homogeneous distribution of cobalt and nitrogen throughout the outer shell is observed. More importantly, the size of Co-MOF sheets can be tuned (Fig. S3†) by changing the concentration of TCCP or reaction temperature.

In the preparation of GO/Co-MOF membranes, the as-exfoliated GO nanosheets and as-obtained Co-MOF nanosheets were dispersed in *N*,*N*-dimethylformamide (DMF) with a respective concentration of 1 mg mL^{-1} before vacuum filtration. Due to numerous residual oxygen-containing functional groups, the GO nanosheets dispersed in DMF are intrinsically electronegative, as confirmed by their measured zeta potential of −52.0 mV (Fig. 1d). Oppositely, Co-MOF is intrinsically electropositive with a zeta potential of +59.1 mV (Fig. 1d). When electropositive Co-MOF is added into the electronegative GO solution, GO nanosheets attach the surfaces of Co-MOF nanosheets. As shown in the vials (inset of Fig. 1d), the precipitates are settled down to the bottom of the container after some time, indicating the electrostatic self-assembly of GO and MOF. Remarkably, unlike physical mixing, the electrostatic self-assembly process can effectively prevent the self-restacking of GO or Co-MOF nanosheets. The flexible freestanding GO/Co-MOF hybrid membranes were obtained through vacuum-assisted filtration of the solutions. For comparison, GO membranes were first fabricated by vacuum filtration of the chemically exfoliated GO nanosheets (Fig. S4†). Fig. 1e–g shows the SEM and TEM images of GO/Co-MOF membrane. A dense surface with some wrinkles can be observed (Fig. 1e). The cross-sectional SEM image of the GO/Co-MOF membrane presents distinct layered structures (Fig. 1f). TEM was employed for further cross-sectional analysis. Fig. 1g shows the corresponding TEM cross-sectional image of as-prepared GO/Co-MOF. Compared to pure GO and MOF membranes (Fig. S5a and b†), the composite membrane exhibits alternating layers of GO and MOF sheets. The high-angle angular dark field scanning TEM and elemental mapping images clearly confirm the alternating layers of GO and Co-MOF sheets (Fig. 1h), demonstrating the effective self-assembly of GO/Co-MOF membrane while the restacking of MOF nanosheets should be restricted very much. The Co-MOF based membrane was denoted as GO/2D-Co-MOF-*x*, where *x* was the mass percentage of Co-MOF in the composite. The XRD patterns for GO/Co-MOF are shown in Fig. 1i. The (002) diffraction peak shifts from 11.3° for GO to 10.2° for GO/2D-Co-MOF-40 membrane, and to a lower 2θ of 9.1° for GO/2D-Co-MOF-60, indicating the insertion of certain amount of MOF between adjacent graphene nanosheets. For high addition amount of GO/2D-Co-MOF-60, the strong diffraction peaks (112), (004) and (006) for Co-MOF are still retained, evidencing the completeness of the nanosheets.

To investigate the compositions of composite membranes, Raman spectroscopy, Fourier transform infrared spectroscopy (FTIR) and X-ray photoelectron spectroscopy (XPS) were performed. The Raman spectra of the samples (Fig. 2a) exhibit two

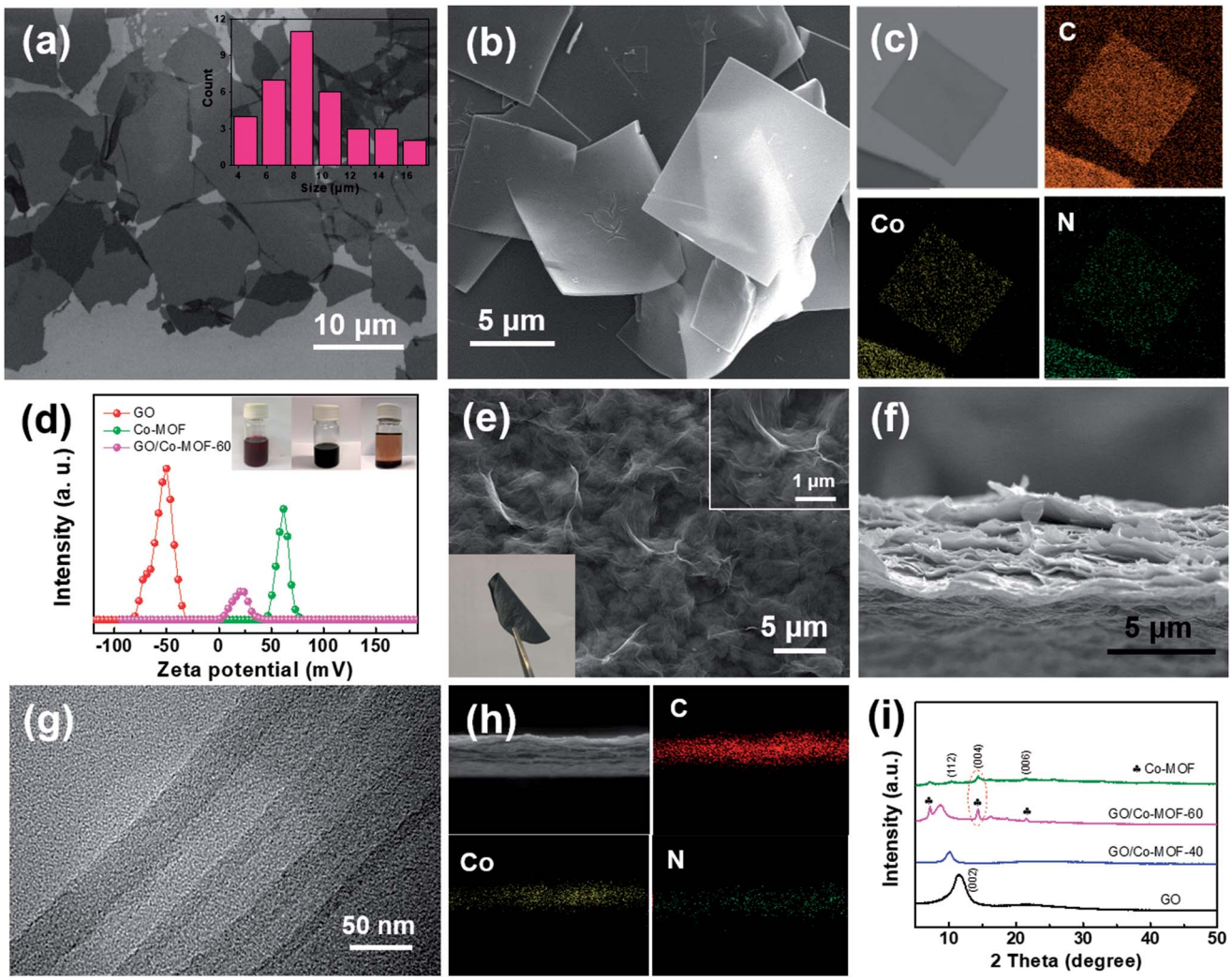

Fig. 1 (a) TEM image of as-exfoliated GO sheets; the inset presents statistical analysis of the diagonal sizes of GO sheets measured in SEM images. (b and c) SEM image and dark-field TEM image of 2D Co-MOF and the corresponding EDX elemental mapping images. (d) Zeta potentials; the inset is the photographs of Co-MOF (left), GO (middle) and GO/Co-MOF (right) solutions. (Panel d reproduced from ref. 16) (e) Top-view SEM image of the GO/2D-Co-MOF-60 composite membrane; the insets show high-resolution top-view SEM image, and flexible, freestanding GO/Co-MOF membranes. (f, g and h) Cross-sectional SEM, TEM and STEM image of the 2D GO/Co-MOF composite membrane and the corresponding EDX elemental mapping images. (i) XRD patterns for as-prepared GO, Co-MOF, GO/2D-Co-MOF-40 and GO/2D-Co-MOF-60 membranes.

remarkable peaks at about 1352 and 1590 cm^{-1}, corresponding to D and G bands, respectively. The G-band is related to the E_{2g}-vibration mode of sp^2 hybridized carbon-based materials, whereas the D-band is assigned to the structural defects or disordering of sp^2 carbon.[22] The calculated peak intensity ratio (I_D/I_G) for hybrid membranes are 0.91 and 0.88, which correspond to GO/2D-Co-MOF-60 and GO/2D-Co-MOF-40 before reduction. The larger value for GO/2D-Co-MOF-60 ($I_D/I_G = 0.91$) is ascribed to the gradually more defects caused by the more additions in MOF sheets.[24] In the FT-IR spectra (Fig. 2b), the peaks located at 1721, 1566, 1430, 1231, and 1080 cm^{-1} are ascribed to C=O, carboxyl O=C–O, epoxy C–O–C, C–O groups, and C=C stretching, respectively.[25] In Co-MOF, the broad band centered at 3460 cm^{-1} and the band located at 2938 cm^{-1} correspond to the O–H stretching vibrations of the physical adsorbed atmospheric moisture/H_2O.[26] More specifically, the peak centered at 3460 cm^{-1} could be assigned to O–H stretching in a water molecule which is adsorbed at the Co site. The peak at 2938 cm^{-1} can be traced to the O–H stretching, the hydrogen in which is further H-bonded to the displaced oxygen connecting to the linker.[27] The bands located at 1676 and 1374 cm^{-1} are ascribed to the symmetric and asymmetric stretching vibrations of C–O bond in TCPP,[28] which could form strong surface complexes with Cs. The bands between the wavenumbers of 614 and 1243 cm^{-1} are attributed to the fingerprint region of terephthalate-based compound.[28] In this region, the strong bands located at 986 and 856 cm^{-1} are attributed to the out-of-plane bending vibration modes of the C–H bond in the benzene ring of the BPY, whereas the band centered at 614 cm^{-1} is due to the stretching vibration of Co–O in the coordinated $Co_2(COO)_4$

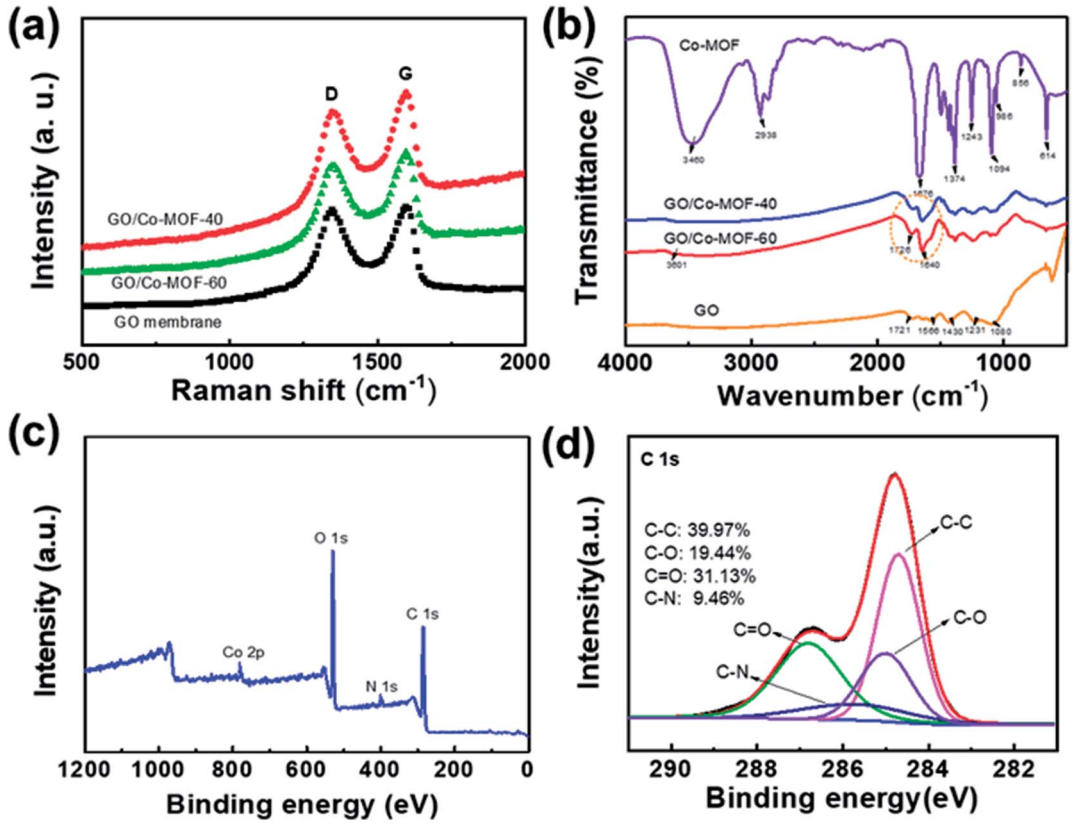

Fig. 2 (a and b) Raman spectra and FT-IR spectra of GO, GO/2D-Co-MOF-40, GO/2D-Co-MOF-60, and Co-MOF. (c) Wide survey XPS spectrum of GO/2D-Co-MOF-60. (d) C 1s spectra for GO/2D-Co-MOF-60.

cluster.[29] For GO/Co-MOF, the O–H stretching shifts from 3460 cm^{-1} of Co-MOF to 3601 cm^{-1}, and the stretching vibrations of C–O at 1676 cm^{-1} shifts to 1640 cm^{-1}. A newly appeared strong peak at 1726 cm^{-1} indicates that the metal oxide clusters are attached to the surface of graphene oxide through oxygen-containing functional groups.[28] Additionally, those functional groups could provide abundant binding sites for the effective removal of Cs^+. A further XPS survey for GO/2D-Co-MOF-60 is presented in Fig. 2c and d. In Fig. S6a,† the Co 2p spectrum shows two characteristic peaks, corresponding to $2p_{3/2}$ and $2p_{1/2}$.[29] The high-resolution N 1s spectrum (Fig. S6b†) indicates that the peak is attributed to pyrrolic-N (398 eV). The high-resolution C 1s peaks as shown in Fig. 2d can be deconvoluted into four peaks, attributing to the following functional groups: ~284.7 eV (C=C/C–C), ~285.5 eV (C–N), ~285.0(C–O) and ~286.9 eV (C=O/O–C=O). All the above-mentioned experiments evidenced that two various oxygen-containing metal-free groups (C–O and C=O) are generated in the composite, which could provide sufficient reactive sites for the binding of Cs^+ during adsorption experiments. We also tested the mechanical properties of the composite membranes as reflected in Fig. S7.† For the composite membranes, the mechanical strength is much higher than that of bare GO. Here we note that the tensile strength value is increased to 102.3 MPa for GO/Co-MOF-60, and 83.4 MPa for GO/Co-MOF-40, compared to the bare GO membrane with lower tensile strength value of 45.1 MPa. Moreover, a Video (S1†) is recorded for the comparison between the stability of GO and GO/Co-MOF in water under ultrasound, which double confirms the excellent flexibility and stability of GO/Co-MOF.

Given that GO/Co-MOF exhibits ultra-high stability and has sufficient reactive sites for Cs^+ binding, herein the sorption mechanism of Cs^+ on the GO/Co-MOF composite membrane from aqueous solution is to be investigated. To maximum the Cs^+ removal efficiency, different important parameters (*e.g.* contact time, reaction temperature, concentrations) were adjusted in detail as follows.

The variation of contact time is a significant parameter in determining the adsorption potential of an adsorbent. Thus, a preliminary study was done on the adsorption of Cs^+ within a time period of 10–240 min at 299 K (Fig. 3a). The adsorbent dose is 3 mg, and the volume of the solution is 10 mL with a Cs^+ concentration of 78 μg mL^{-1}, and pH = 7. The maximum Cs^+ removal efficiency for GO/2D-Co-MOF-40 membranes is 45.6% after 240 min. Surprisingly, when the GO/2D-Co-MOF-60 composite membranes are employed as adsorbents, the uptake of Cs^+ increases significantly in the first 20 min and reaches a plateau within 60 min. The best removal efficiency for GO/2D-Co-MOF-60 membranes occurs at 240 min, with a value of 65.02%. The uptake quantity of Cs^+ on GO/Co-MOF samples is shown in Fig. S8a,† and the maximum sorption capacity q_e of Cs^+ on GO/Co-MOF is 168.79 mg g^{-1}. Although the value is

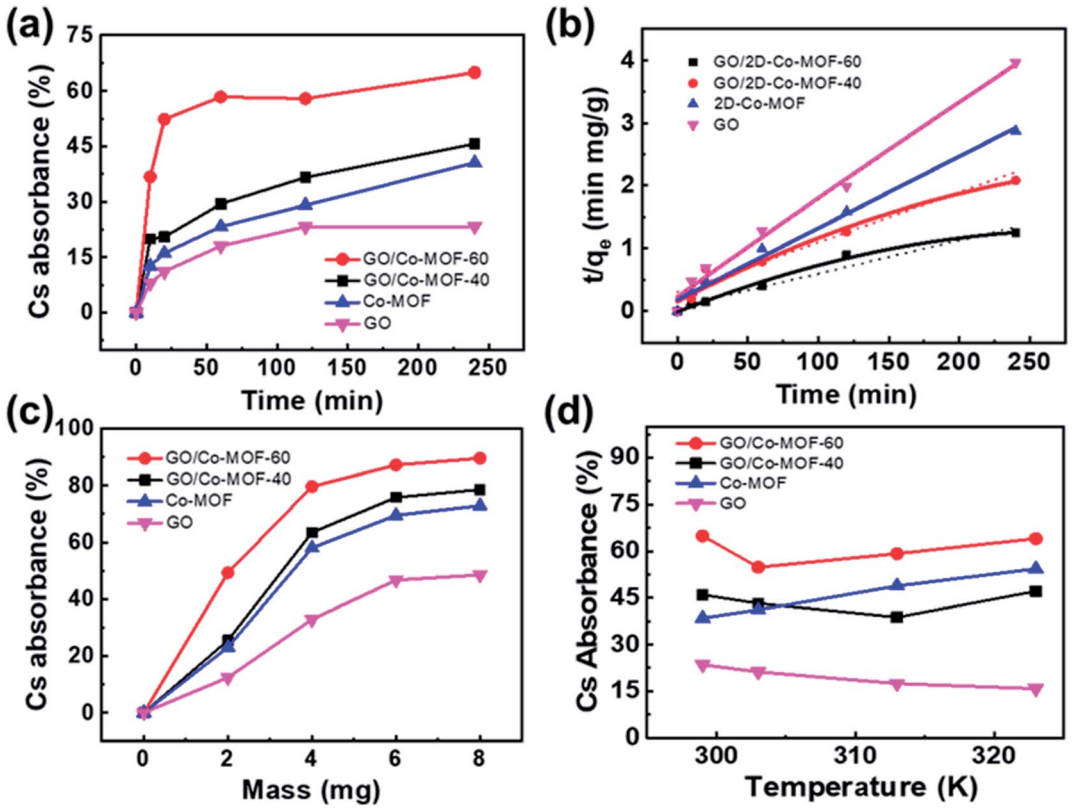

Fig. 3 (a) Effects of contact time on the adsorption of Cs^+ on GO/Co-MOF membranes; (b) the time-dependent sorption pseudo-second-order kinetic plots (solid lines) of Cs^+ removal on GO, Co-MOF, GO/2D-Co-MOF-40 and GO/2D-Co-MOF-60. (c) Effect of adsorbent dosage on the adsorption of Cs^+ on GO/Co-MOF membranes. (d) Effects of temperature on the adsorption of Cs^+ on GO/Co-MOF membranes.

lower than that of 3D uranyl organic framework (432 mg g^{-1}), it is higher than that of MOF/KNiFC (153 mg g^{-1}).[30,31] It is noted that the Cs^+ removal efficiency of membranes changing from GO/2D-Co-MOF-40 to GO/2D-Co-MOF-60, that is, the value increases with increasing the concentration of surface-active sites. For comparison, the influence of contact time on the sorption of Cs^+ onto pure MOF and GO were also investigated (Fig. 3a). For pure MOF, the removal of Cs^+ increases rapidly within the first 10 min, and slowly increases afterwards till 240 min. The enhanced sorption suggests that the 2D Co-MOF nanomaterial provides abundant active sites to bind Cs^+. For GO, the removal of Cs^+ become close to saturation within 150 min, and the growing tendency slows down with the increasing of contact time. To extract the interaction mechanism in details, the sorption kinetics is fitted by the pseudo-first-order model and pseudo-second-order model,[32] which are described as follows:

$$q_t = q_e(1 - e^{-k_1 t}) \quad (3)$$

$$q_t = \frac{k_2 t q_e^2}{1 + q_e t k_2} \quad (4)$$

where q_e (mg g^{-1}) and q_t (mg g^{-1}) are the amounts of absorbate uptake per mass of adsorbent at equilibrium and at time t (min), respectively; k_1 (1/min) and k_2 (g (mg min)$^{-1}$) are the rate constant of the pseudo-first-order equation and the pseudo-second-order equation, respectively. The pseudo-second-order model fitting calculation is presented in Fig. 3b and the relevant kinetic parameters are tabulated in Table S1.† According to the linearity of fitting R^2 and q_e values, it is clear that the Cs^+ sorption on Co-MOF or GO/2D-Co-MOF-60 can be better described by the pseudo-second-order model, which demonstrates that the Cs^+ removal behavior is dominated by a chemical sorption process in the composite membranes, especially in those with high contents of Co-MOF.

The effect of adsorbent dosage on the adsorption process is also investigated, as shown in Fig. 3c and S8b.† The dosage of membranes is set at 2, 4, 6, and 8 mg. Other experimental conditions are set as follows: temperature 299 K, contact time 240 min, volume of the solution 10 mL, initial Cs^+ solution 78 μg mL^{-1} and pH = 7. For the GO/Co-MOF membranes, the uptake of Cs^+ increases at low adsorbent weight and reaches a plateau at high adsorbent weight, which could be attributed to the exposure of accessible surface-active sites for adsorption. In the very beginning of adsorption, sufficient active sites are available for Cs^+ uptake. As the adsorbent mass increases, the active sites gradually become saturated and achieve dynamic equilibrium, suggesting that there is an optimal adsorbent dosage for the Cs^+ removal from the aqueous solution. For the GO/2D-Co-MOF-60 adsorbent, an adsorption percentage of 88.4% is achieved under a weight of 8 mg. It is noted that when the adsorbent weight is 2 mg, the Cs^+ removal efficiency for GO/

2D-Co-MOF-60 membranes is almost 2 times higher than that of GO/2D-Co-MOF-40 membranes. However, the value decreases to 1.15 times when the adsorbent weight increases to 8 mg. Thus, compared to GO/2D-Co-MOF-40, the GO/2D-Co-MOF-60 membrane is more advantageous at a lower adsorbent weight for Cs^+ removal. Similarly, for pure GO and Co-MOF, the sorption percentage increases with increasing sample dosage, but the overall adsorption capacities of pure GO and Co-MOF samples are lower than that of composite membranes. It is observed that the q_e values decrease with the adsorbent weight increasing from 4 mg to 8 mg (Fig. S8b†). The decrease of q_e value might be caused by the competition between sorption sites, which can reduce their complexation ability to heavy metal ions of Cs^+ at high adsorbent dosage. Thus, one could speculate that more sorption sites are available for binding Cs^+ to enhance the Cs^+ removal efficiency at low adsorbent weight. However, the competition between the active sites at high adsorbent dosage may greatly reduce the free binding sites, which thereby results in the slow increase of Cs^+ removal.

The effects of temperature on the removal of Cs^+ are investigated at 299, 303, 313, and 323 K (Fig. 3d). Other experimental conditions are kept the same: contact time 240 min, adsorbent dose 3 mg, volume of the solution 10 mL, initial Cs^+ solution 78 μg mL^{-1} and pH 7. As shown in Fig. 3d and S8c,† the Cs^+ removal efficiency and/or capacity for GO/2D-Co-MOF-60 is always higher than that for GO/2D-Co-MOF-40 membranes. The sorption of Cs^+ on Co-MOF significantly increases with increasing temperature, indicating that a higher temperature is beneficial for Cs^+ sorption on MOF samples. For GO samples, however, an opposite result is found due to the partial reduction occurred in the GO at elevated temperatures.[21] Interestingly, the variation of adsorption efficiencies is similar for both composite membranes, that is, it first decreases and then increase. For the GO/2D-Co-MOF-40 members, the reduction of GO leads to a reduced adsorption efficiency in the beginning, while a higher temperature promotes the removal of Cs^+ by MOF. The GO/2D-Co-MOF-60 exhibits a decrease in absorbance efficiency from 299 to 303 K. The value rapidly increases from 303 to 323 K, evidencing that the high addition amount of Co-MOF in GO/2D-Co-MOF-60 composite membrane plays a crucial role in the adsorption efficiency. The q_{max} of Cs^+ on GO/2D-Co-MOF-60 (192.14 mg g^{-1}) is much higher than those of other materials, suggesting that the GO/2D-Co-MOF-60 is a suitable and promising material for the efficient elimination of Cs^+ (Fig. S8a–S8c†).

To evaluate the stability of spent GO/Co-MOF adsorbent, SEM analysis is carried out on the fresh and used adsorbents (Fig. S9†). The rough surfaces (Fig. S9b†) as well as their EDS mapping (Fig. S10†) further confirm the adsorption of Cs^+ on the GO/Co-MOF adsorbent. Meanwhile, the region marked in a green square in Fig. S9f† indicates the structural integrity of Co-MOF after Cs^+ adsorption. Fig. 4a shows the XPS spectra of GO/2D-Co-MOF-60 before and after Cs^+ sorption. Two new peaks attributed to Cs 3d appear after Cs^+ sorption, confirming that Cs^+ is successfully absorbed on the GO/2D-Co-MOF-60 surfaces (also shown in Fig. S9b†). In the high-resolution Cs 3d spectrum (Fig. 4b), the peaks at the binding energies of 738.2 and 724.1 eV correspond to Cs $3d_{3/2}$ and Cs $3d_{5/2}$, respectively. Fig. 4c reveals the high-resolution C 1s spectrum of GO/2D-Co-MOF-60 after Cs^+ uptake, which could be divided into four components including C–C (284.7 eV), C–N (285.5 eV) C–O (286.82) and C=O (286.7 eV).[32] Compared to the spectrum of C 1s before Cs^+ sorption (Fig. 2d), it is clear that the peak positions of C–O and C=O shift significantly after Cs^+ sorption. For C–O, the peak position shifts from 285.0 to 286.82 eV after Cs^+ sorption. Moreover, for C=O, the peak position changes from 286.9 to 286.7 eV after Cs^+ sorption. And, the peak areas of C–O, C=O and C–C change significantly after Cs^+ sorption.[24] In specific, the peak area of C–O decreases from 19.44% to 13.60%, and that of C=O decreases from 31.13% to 28.15%, while that of C–C increases from 39.97% to 48.74%. The results indicate that the chemical environment of those oxygen containing functional groups (*i.e.*, C=O and C–O) change and Cs^+ might form surface complexation with C=O and C–O of GO/2D-Co-MOF-60 during the reaction processes (Fig. 4d). Based on the results (Fig. 3b), the dominant interaction mechanisms between Cs^+ and the composite membranes could be chemical adsorption and electrostatic interaction, as illustrated in Fig. 4e. For the bare Co-MOF, physical sorption dominates in the removal of Cs^+. The large pores (diameter ~10 Å) in the crystal structure of Co-MOF nanosheets could effectively hold the Cs^+ ions (ion radius ~1.67 Å), and the stable connection between oxygen-containing groups and Co in MOF hinder the chemical adsorption of Cs^+ (Fig. 4f).[33] For the GO membranes, it has also been reported that the in-plane oxygen functional groups limit the diffusion of water molecules into the graphene nanochannels due to hydrogen bonds,[34] which further rejects the diffusion of Cs^+ in solutions into the GO channels, as illustrated in Fig. 4g.[26] Therefore, the poor Cs^+ adsorption is found in GO membranes (Fig. 3a, c and d). For the GO/Co-MOF membranes with sandwiched composite structures, the interfaces between Co-MOF and GO may effectively eliminate the hydrogen bond at the GO surfaces, thus facilitating the permeation and adsorption of Cs^+ with oxygen-containing groups in GO. Besides, the GO sheets also activate the outer surfaces of MOF. Thus, the interaction mechanism of Cs^+ in Co-MOF is better described as chemical adsorption instead of the aforementioned physical sorption. The chemical adsorption is also demonstrated based on the FT-IR spectra of GO/Co-MOF with new peaks marked in brown circles (Fig. 2b). Thus, the synergistic effect between GO and Co-MOF provides a high specific surface area and a facilitate 'corridor' for ion transfer and adsorption.

The cycle pattern of adsorption–desorption–drying–adsorption was used to investigate the reusing performance of membrane materials. We used distilled water, 1 mol L^{-1} HNO_3 solution and 0.5 mol L^{-1} NH_4NO_3 solution to clean the membranes successively which were used subsequently for repeated absorption experiment after drying. Thus, a similar study was done on the adsorption of Cs^+ within a time period of 240 min at 299 K. The adsorbent dose is 3 mg, and the volume of the solution is 10 mL with a Cs^+ concentration of 78 μg mL^{-1}, and pH = 7. The maximum Cs^+ removal efficiencies of the GO/2D-Co-MOF-60 membranes are 65.02%, 60.1%, 57.4%, and 55.7% for the multiple regeneration cycle performance of four

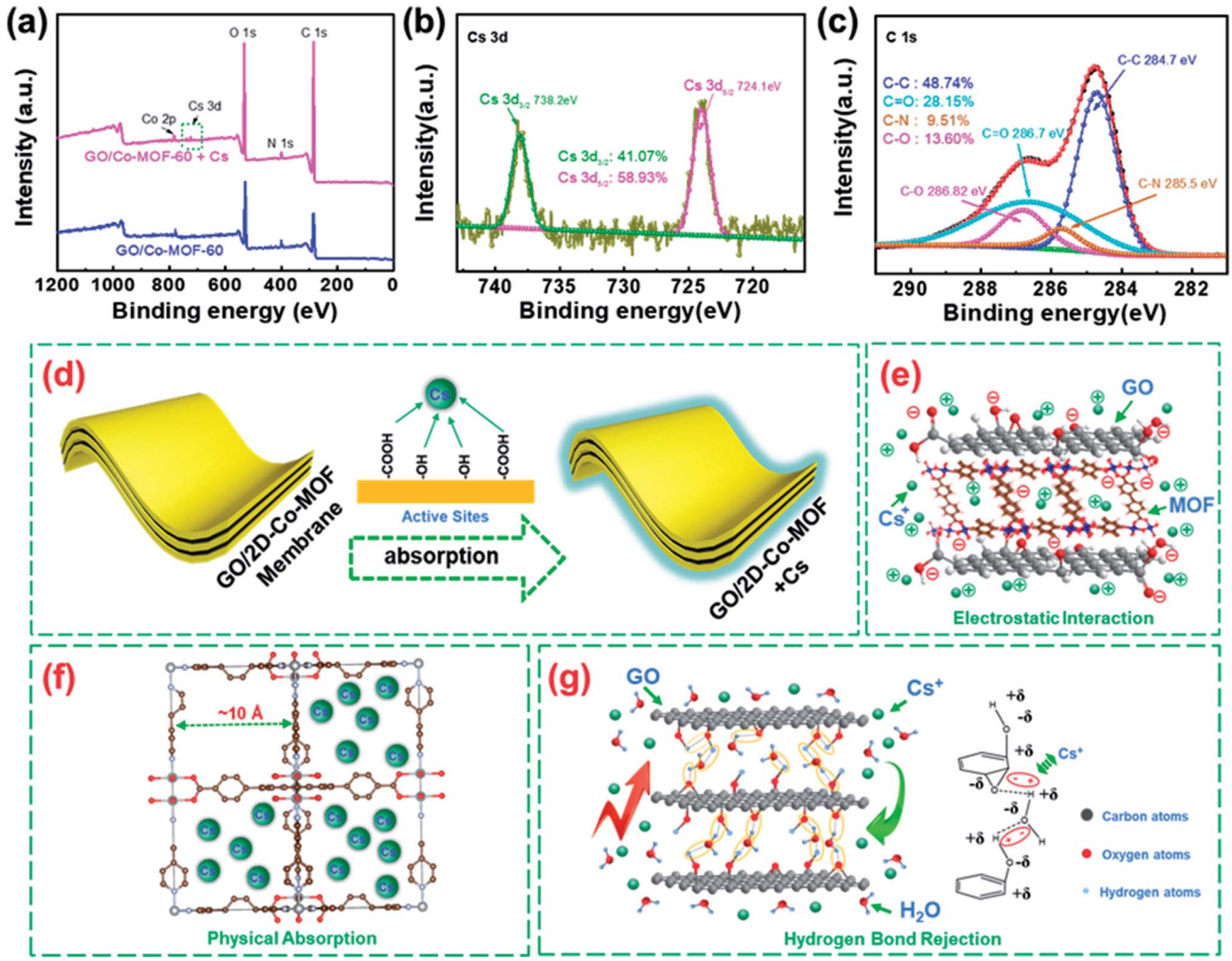

Fig. 4 (a) The XPS spectra of GO/Co-MOF before and after Cs^+ sorption; (b) the Cs 3d XPS spectrum of GO/Co-MOF after Cs^+ sorption; (c) the C 1s XPS spectrum of GO/Co-MOF after Cs^+ sorption; (d) sorption mechanism of Cs^+ on GO/Co-MOF samples; (e) schematic of mechanisms of sorption reaction in GO/Co-MOF composite membranes; (f) Schematic of mechanisms of sorption reaction in Co-MOF; (g) Schematic of mechanisms of sorption reaction in GO membranes.

times adsorption from the first adsorption to the fourth adsorption repeatedly. Obviously, the uptake of Cs^+ on the composite membranes doesn't decrease significantly in the repeated cycle using and the value kept above 55%. For comparison, the repeated sorption of Cs^+ onto pure MOF and GO were also investigated. For pure MOF, the removal efficiency of Cs^+ decreases rapidly from 36.4% to 17.4% within four times sorption, which could be caused by the gradual saturation physical sorption. The GO membranes have the most stable removal-efficiency from 21.1% to 15.4% with the fourth-time repeated absorption. The high efficient removal efficiency might result from gradual consuming in-plane oxygen functional groups, which promotes the diffusion of water molecules into the graphene nano-channels.

4. Conclusions

We have successfully synthesized a novel self-assembled membrane consisting of 2D-metal–organic frameworks and graphene oxides through a simple high-yield facile filtration method. The synthesized GO/Co-MOF membranes have abundant oxygen-containing functional groups (such as C–O, C=O), which were confirmed by FT-IR and XPS analyses. Batch experimental results suggested that the GO/2D-Co-MOF-60 adsorbent had an optimal removal capacity of Cs^+ (192.14 mg g^{-1}) under a contact time of 4 hours and an adsorbent dose of 2 mg. Compared with GO/2D-Co-MOF-40 membrane, bare GO and Co-MOF samples, the GO/2D-Co-MOF-60 membrane exhibited a much better Cs^+ removal efficiency, which was more obvious in the very beginning of Cs^+ adsorption and at a lower adsorbent dosage. This work demonstrates that GO/Co-MOF composite membranes are promising sorbent candidates for nuclear waste remediation.

Conflicts of interest

There are no conflicts to declare.

Acknowledgements

This work was supported by National Key R&D Program of China (Grant No. 2016YFC1402504), the National Natural Science Foundation of China (51272110 and 51771123), the Shenzhen Peacock Innovation Project (Grant No. KQJSCX20170327151307811). Dr G. C. Shan gratefully thank Prof. Way Kuo, President of City University of Hong Kong, for stimulating discussions and suggestions about the reliability and unwanted radioactive waste of nuclear energy.

References

1 X. X. Wang, S. Q. Yu, Y. H. Wu, H. W. Pang, S. J. Yu, Z. S. Chen, J. Hou, A. Alsaedi, T. Hayat and S. H. Wang, The synergistic elimination of uranium (VI) species from aqueous solution using bi-functional nanocomposite of carbon sphere and layered double hydroxide, *Chem. Eng. J.*, 2018, **342**(15), 321–330.

2 Y. L. Wang, Z. Y. Liu, Y. X. Li, Z. L. Bai, W. Liu, Y. X. Wang, X. M. Xu, C. L. Xiao, D. P. Sheng, J. Diwu, J. Su, Z. F. Chai, T. E. Albrecht-Schmitt and S. Wang, Umbellate distortions of the uranyl coordination environment result in a stable and porous polycatenated framework that can effectively remove cesium from aqueous solutions, *J. Am. Chem. Soc.*, 2015, **137**(19), 6144.

3 M. Manolopoulou, E. Vagena, S. Stoulos, A. Ioannodou and C. Papastefanou, Radioiodine and radiocesium in Thessaloniki, Northern Greece due to the Fukushima nuclear accident, *J. Environ. Radioact.*, 2011, **102**(8), 796.

4 K. Shakir, M. Sohsah and M. Soliman, Removal of cesium from aqueous solutions and radioactive waste simulants by coprecipitate flotation, *Sep. Purif. Technol.*, 2007, **54**(3), 373.

5 M. V. Balarama Krishna, S. V. Rao, J. Arunachalam, M. S. Murali, K. Surendra Kumar and V. K. Manchanda, Removal of ^{137}Cs and ^{90}Sr from actual low-level radioactive waste solutions using moss as a phyto-sorbent, *Sep. Purif. Technol.*, 2004, **38**(2), 149.

6 S. Singh, S. Eapen, V. Thorat, C. P. Kaushik, K. Raj and S. F. D'Souza, Phytoremediation of ^{137}cesium and ^{90}strontium from solutions and low level nuclear waste by Vetiveria zizanioides, *Ecotoxicol. Environ. Saf.*, 2008, **69**(2), 306.

7 M. D. Neville, C. P. Jones and A. D. Turner, The EIX process for radioactive waste treatment, *Prog. Nucl. Energy*, 1998, **32**(3), 397.

8 G. Zhao, X. Huang, Z. Tang, Q. Huang, F. Niu and X. Wang, Polymer-based nanocomposites for heavy metal ions removal from aqueous solution: a review, *Polym. Chem.*, 2018, **9**, 3562.

9 J. Li, X. Wang, G. Zhao, C. Chen, Z. Chai, A. Alsaedi, T. Hayat and X. Wang, Metal-organic framework-based materials: superior adsorbents for the capture of toxic and radioactive metal ions, *Chem. Soc. Rev.*, 2018, **47**, 2322.

10 P. Gu, S. Zhang, X. Li, X. Wang, T. Wen, R. Jehan, A. Alsaedi, T. Hayat and X. Wang, Recent advances in layered double hydroxide-based nanomaterials for the removal of radionuclides from aqueous solution, *Environ. Pollut.*, 2018, **240**, 493.

11 Y. Wu, H. Pang, W. Yao, X. Wang, S. Yu, Z. Yu and X. Wang, Synthesis of rod-like metal-organic framework (MOF-5) nanomaterial for efficient removal of U(VI): batch experiments and spectroscopy study, *Sci. Bull.*, 2018, **63**(13), 831.

12 C. Zhang, X. Li, Z. Chen, T. Wen, S. Huang, T. Hayat, A. Alsaedi and X. Wang, Synthesis of ordered mesoporous carbonaceous materials and their highly efficient capture of uranium from solutions, *Sci. China: Chem.*, 2018, **61**(3), 281.

13 W. Yao, Y. Wu, H. Pang, X. Wang, S. Yu and X. Wang, *In situ* reduction synthesis of manganese dioxide@polypyrrole core/shell nanomaterial for highly efficient enrichment of U(VI) and Eu(III), *Sci. China: Chem.*, 2018, **61**(7), 812.

14 K. Yamamoto, Y. Sakata, Y. Nohara, Y. Takahashi and T. Tatsumi, Organic-inorganic composite zeolites containing organic frameworks, *Science*, 2003, **300**(5618), 470.

15 G. Férey, Hybrid porous solids: past, present, future, *Chem. Soc. Rev.*, 2008, **37**, 191.

16 J. Cheng, S. Chen, D. Chen, L. Dong, J. Wang, T. Zhang, T. Jiao, B. Liu, H. Wang, J.-J. Kai, D. Zhang, G. Zheng, L. Zhi, F. Kang and W. J. Zhang, *J. Mater. Chem. A*, 2018, **6**(41), 20254.

17 U. Mueller, M. Schubert, F. Teich, H. Puetter, K. Schierle-Arndta and J. Pastréa, Metal-organic frameworks-prospective industrial applications, *J. Mater. Chem.*, 2006, **16**(7), 626.

18 L. Fan, M. Deng, C. Lin, C. Xu, Y. Liu, Z. Shi, Y. Wang, Z. Xu, L. Li and M. He, A multifunctional composite Fe3O4/MOF/L-cysteine for removal, magnetic solid phase extraction and fluorescence sensing of Cd(II), *RSC Adv.*, 2018, **8**, 10561.

19 B. Aguila, D. Banerjee, Z. Nie, Y. Shin, S. Ma and P. K. Thallapally, Selective removal of cesium and strontium using porous frameworks from high level nuclear waste, *Chem. Commun.*, 2016, **52**(35), 5940.

20 Z. Y. Gu, C. X. Yang, N. A. Chang and X. P. Yan, Metal–organic frameworks for analytical chemistry: from sample collection to chromatographic separation, *Acc. Chem. Res.*, 2012, **45**(5), 734.

21 Z. Han, K. Zhan, X. Y. Wang, G. P. Zheng and J. H. Yang, Scalable Piezoelectricity in Graphene Oxide Papers Tuned by Hydrogen Bonds, *Adv. Electron. Mater.*, 2016, **2**(10), 1600224.

22 P. Kumar, F. Shahzad, S. Yu, S. M. Hong, Y. H. Kim and C. M. Koo, Large-area reduced graphene oxide thin film with excellent thermal conductivity and electromagnetic interference shielding effectiveness, *Carbon*, 2015, **94**, 494.

23 D. L. Zhang, Y. H. Zhu, L. M. Liu, X. R. Ying, C. E. Hsiung, R. Sougrat, K. Li and Y. Han, Atomic-resolution transmission electron microscopy of electron beam-sensitive crystalline materials, *Science*, 2018, **359**(6376), 675–684.

24 X. Lin, X. Shen, Q. Zheng, N. Yousefi, L. Ye, Y. W. Mai and J. K. Kim, Fabrication of highly-aligned, conductive, and

strong graphene papers using ultralarge graphene oxide sheets, *ACS Nano*, 2012, **6**(12), 10708.

25 J. Wang, Z. Chen and B. Chen, Adsorption of polycyclic aromatic hydrocarbons by graphene and graphene oxide nanosheets, *Environ. Sci. Technol.*, 2014, **48**(9), 4817.

26 Y. F. Feng, H. Jiang, M. Chen and Y. R. Wang, Construction of an interpenetrated MOF-5 with high mesoporosity for hydrogen storage at low pressure, *Powder Technol.*, 2013, **249**(11), 38.

27 Y. Ming, J. Purewal, J. Yang, C. C. Xu, R. Soltis, J. Warner, M. Veenstra, M. Gaab, U. Müller and D. J. Siege, Kinetic stability of MOF-5 in humid environments: impact of powder densification, humidity level, and exposure time, *Langmuir*, 2015, **31**(17), 4988.

28 Z. P. Wu, M. X. Wang, L. J. Zhou, Z. L. Yin, J. Tan, J. L. Zhang and Q. Y. Chen, Framework-solvent interactional mechanism and effect of NMP/DMF on solvothermal synthesis of $[Zn_4O(BDC)_3]_8$, *Trans. Nonferrous Met. Soc. China*, 2014, **24**(11), 3722.

29 F. F. Cao, M. T. Zhao, Y. F. Yu, B. Chen, Y. Huang, J. Yang, X. H. Cao, Q. P. Lu, X. Zhang, Z. C. Zhang, C. L. Tan and H. Zhang, Synthesis of two-dimensional $CoS_{1.097}$/nitrogen-doped carbon nanocomposites using metal-organic framework nanosheets as precursors for supercapacitor application, *J. Am. Chem. Soc.*, 2016, **138**(22), 6924.

30 Y. Wang, Z. Liu, Y. Li, Z. Bai, W. Liu, Y. Wang, X. Xu, C. Xiao, D. Sheng and J. Diwu, Umbellate distortions of the uranyl coordination environment result in a stable and porous polycatenated framework that can effectively remove cesium from aqueous solutions, *J. Am. Chem. Soc.*, 2015, **137**, 6144.

31 S. Naeimi and H. Faghihian, Performance of novel adsorbent prepared by magnetic metal-organic framework (MOF) modified by potassium nickel hexacyanoferrate for removal of Cs^+ from aqueous solution, *Sep. Purif. Technol.*, 2017, **175**, 255.

32 Y. D. Zou, P. Y. Wang, W. Yao, X. X. Wang, Y. H. Liu, D. X. Yang, L. D. Wang, J. Hou, A. Alsaedi, T. Hayat and X. K. Wang, Synergistic immobilization of UO_2^{2+} by novel graphitic carbon nitride@layered double hydroxide nanocomposites from wastewater, *Chem. Eng. J.*, 2017, **330**, 573.

33 Z. M. Hao, X. Z. Song, M. Zhu, X. Meng, S. N. Zhao, S. Q. Su, W. T. Yang, S. Y. Song and H. J. Zhang, One-dimensional channel-structured Eu-MOF for sensing small organic molecules and Cu^{2+} ion, *J. Mater. Chem. A*, 2013, **1**, 11043.

34 J. Y. Chong, B. Wang and K. Li, Water transport through graphene oxide membranes: the roles of driving forces, *Chem. Commun.*, 2018, **54**(20), 2554.